

Performance improvement of CSP particle receivers by depositing spinel absorber coatings

Meryem Farchado^{a,b,*}, Gema San Vicente^a, Naia Barandica^{a,b}, Florian Sutter^c, Gözde Alkan^d, Daniel Sánchez-Señorán^e, Ángel Morales^a

^a CIEMAT-PSA. Materials for Concentrating Solar Thermal Technologies Unit, Avenida Complutense 40, Madrid, 28040, Spain

^b Universidad Autónoma de Madrid. Ciudad Universitaria de Cantoblanco, Madrid, 28049, Spain

^c Institute of Solar Research, German Aerospace Center (DLR), Calle Doctor Carracido 42-1, Almería, 04005, Spain

^d Institute of Materials Research, German Aerospace Center (DLR), Cologne, 51147, Germany

^e CIEMAT-PSA. Point Focus Solar Thermal Technologies Unit, Avenida Complutense 40, Madrid, 28040, Spain

ARTICLE INFO

Keywords:

Solid particle technology
 Spinel coating
 Solar absorber
 Abrasion resistance
 Thermal-stability
 Dip-coating
 CSP

ABSTRACT

The challenging development/modification of particles to meet the requirements of thermal stability, high absorptance and mechanical resistance with minimal economical cost is a key point to attain for the next particle receivers of concentrated solar power plants. The properties of the particles influence the performance of the system, since the concentrated solar radiation is absorbed and stored in these solid materials. In this work, resulting from the studies carried out within the HORIZON 2020 COMPASSCO2 project, the deposition of black-coloured transition-metal oxides with spinel-like structure coatings on different particles is proven. Five different particles (state-of-the-art and innovative) developed by Saint-Gobain have been coated, studied and compared. The coating deposition was adapted to the dip-coating methodology, ensuring high and good reproducibility. The composition of solid particles as well as the composition of the precursor solution, the curing methodology and the number of deposited spinel layers demonstrate that they have a great influence on the solar absorptance value and the abrasion resistance. Therefore, it is essential to find the perfect balance between all these different parameters in order to achieve the best performance of the particles. The addition of silica nanoparticles in the precursor solution provides rougher layers with enhanced absorptance, up to 0.980, on newly developed particles with excellent thermal stability and abrasion resistance.

1. Introduction

The current energy crisis and climate change have greatly inspired the search for alternatives to traditional fossil fuels. These alternatives will contribute to achieve the goal of the European Union of decarbonising the power sector by 2050 [1] by increasing the use of more efficient energy conversion systems and renewable energy sources. Solar energy, concretely, the concentrated solar power (CSP) systems, stand out as indisputable candidates given their sustainability (respect for the environment), affordability (abundance) and reliability. During the last decades, increasing interest has been shown in improving current commercial CSP plants (390 °C for thermo-oil and 560 °C for molten salt) [2–6] taking into account the weakness of this technology due to the freezing and decomposition behaviour of the working fluid outside the useable temperature range. Nowadays, CSP systems based on

particle technology are a growing field where solid particles used as receivers in CSP plants are potential candidates to overcome current working temperature limits, given their high temperature stability (close to 1000 °C) and their high flexibility in terms of the selection of temperature levels [5,7]. Furthermore, these solid particles are also preferred as a thermal storage medium, resulting in this way in a reduction in the complexity and costs of the system [6,8,9]. Therefore, in this new concept, solid particles will be responsible for absorbing (serving the particle medium as a solar absorber and heat transfer fluid (HTF)) and storing (serving as thermal energy storage (TES) material) [10]. In fact, since the radiation is directly absorbed by the particle receivers, flux restrictions and heat transfer resistance linked to indirect heating across the tube walls are ruled out [4,11]. Definitely, since the concentrated solar radiation is absorbed in the particles, the receiver overall efficiency is crucially conditioned by the optical radiative

* Corresponding author. CIEMAT-PSA. Materials for Concentrating Solar Thermal Technologies Unit. Avenida Complutense 40, Madrid, 28040, Spain
 E-mail address: meryem.farchado@ciemat.es (M. Farchado).

<https://doi.org/10.1016/j.solmat.2023.112681>

Received 28 July 2023; Received in revised form 10 November 2023; Accepted 10 December 2023

Available online 26 December 2023

0927-0248/© 2023 The Authors. Published by Elsevier B.V. This is an open access article under the CC BY-NC license (<http://creativecommons.org/licenses/by-nc/4.0/>).

properties of this solid material; it is more interesting to maximise the solar absorptance value even though it implies an increase in the thermal emittance value as well. This means that a good solar material is whose solar absorptance is high, although its thermal emittance is high [12].

Based on the important role that solid particles play in CSP technologies, it is mandatory for these solid materials to achieve several tempting properties such as high packing density, high heat capacity, resistance to high-temperature oxidation and erosion, resistance to sintering and agglomeration, high solar absorptance, relatively low thermal emittance, low cost, and wide availability [4,13]. Several research studies are focused on the manufacturing of suitable particles with the best performance [14] and environmentally friendly (from recycled material) [15].

The solid particles mainly employed in a particle receiver are ceramic-based materials (alumina, silica, silicon carbide, zirconia and proppants) [16,17]. The most used are sintered bauxite-type ceramic proppants [18,19]. The resistance of these materials, which correlates with their porosity and therefore with their density, determines the lifetime and the maximum closure stress [20]. Based on their density and strength, which are related to the alumina content, ceramic proppants can be categorised into three groups: lightweight ceramics (LWC) containing 45–50 % of alumina, intermediate density ceramics (IDC) enclosing 70–75 % of alumina and high density ceramics (HSC) composed of 80–85 % of alumina [21]. In general, proppants are strong, resistant to sintering under pressure, non-corrosive and have a measured solar weighted absorptance greater than 90 %. However, these bauxite-type proppants showed limited optical performance after thermal exposure in several studies performed [19,22,23], demonstrating the need to improve their surface to overcome these durability drawbacks. To achieve this goal, modification of the surface of the particles by applying a durable solar absorber coating is considered a promising solution. Spinel-type transition metal oxides are commonly used for the design of spectrally selective absorber coatings (SSACs) in solar energy conversion field. These materials present a high ability to absorb all incident solar radiation with minimal heat losses and their high thermal stability [24–30]. Few studies have been conducted on solar absorber coatings applied to solid particles given the novelty of the particle receiver concept [22,23,31]. However, in recent decades, the interest in improving the reliability and long-term performance stability of solar receivers has acquired increasing importance; resulting in several publications on this matter [32–35]. Different methodologies for the deposition of coatings on solid particles have been proposed in previous researches, such as mixing particles with spinel powders by a resonant acoustic mixer [18] or ball milling [36]. Other authors have proposed the calcination of high-viscous gel containing transition metal oxides with a chelating agent and sand/bauxite to obtain a final spinel powder [37,38]. Spinels of three metals (Cu, Mn, Fe, and Cu, Cr, Mn) and of two metals (Mn, Fe, and Cu, Mn) have been prepared using these methodologies. With these materials and methods, the highest solar absorptance value reported was 0.92 [18].

Within the HORIZON 2020 COMPASCO2 project, the integration of the CSP particle system into highly efficient CO₂ Brayton power cycles is pursued for electricity production. Therefore, the design, development and test of high-performance particles for CSP receivers are primordial tasks to address. In this work, the advances reached in solid particle materials to improve their current optical properties, high-temperature stability and abrasion resistance with low cost are presented. To this end, different kinds of particles developed by Saint-Gobain have been coated with new designed spinel coatings using an optimised process of depositing and sintering. This work provides an innovative way to apply coatings on particles with a methodology adapted from the dip coating principle, guaranteeing the simplicity, easy-scalability, reproducibility, flexibility and cost-effectiveness typical of this technique. The application of Cu, Mn and Co spinels on particles to increase solar absorptance has not been previously reported. All particles studied have been

optically measured both in the as-received state and after coating. A complete study of abrasion resistance, thermal stability and characterisation by scanning electron microscopy (SEM) has been performed for the spinel-coated solid particle with the best optical performance.

2. Materials and experimental methodology

2.1. Sample preparation

Four “state-of-the-art” (S.O.A.) particles with mesh sizes of 16/30 (BauxLite/BL) and 30/50 (BauxLite/BL, Sintered Bauxite/SB and Interprop/IP) presented in SolarPACES 2021 Conference [39] and a new generation of solid particles (Gen3) with a size between 0.6 and 1.2 mm developed by Saint-Gobain were studied. They were coated with dark precursor solutions by chemical deposition under atmospheric conditions of humidity (50–60 %) and at room temperature (22 °C). Taking into account the small size of the particles, a new methodology adapted to the principle of dip-coating has been designed to coat them. This new application method consists of adding the precursor solution to 50 g of particles, which are located in a funnel with a paper filter, until they are totally covered. The precursor solution is then drained by gravity and the resulting coated particles are introduced into the oven at high temperature (600 °C or 1000 °C depending on the chosen heat treatment) for curing. Two different heat treatment methodologies (Method 1 and Method 2) have been studied and compared. A maximum of five layers were applied to the solid particles studied, incorporating a thermal treatment between the deposition of each coating. The experimental procedure followed is schematised in Fig. 1.

Two precursor solutions were prepared for the experiments shown in this manuscript: CuCoMnO_x (Sol B) and SiO₂/CuCoMnO_x (Sol A). Both solutions were prepared by dissolving in absolute ethanol the precursors of copper nitrate (Sigma Aldrich, 98–103 %), cobalt nitrate (PRS Panreac, 98 %) and manganese nitrate (PRS Panreac, 98 %) in a molar ratio of 1:0.6:1 and adding a complexing agent and a wetting additive to improve film adhesion [40]. 15 % colloidal silica (Aerosil® 792) was incorporated into Sol A, giving an interesting roughness to the coating. Then, the only difference between both precursor solutions is the presence (Sol A) or absence (Sol B) of silica nanoparticles, showing in both cases long-term stability, ensuring in this way reproducible and reliable absorber deposition.

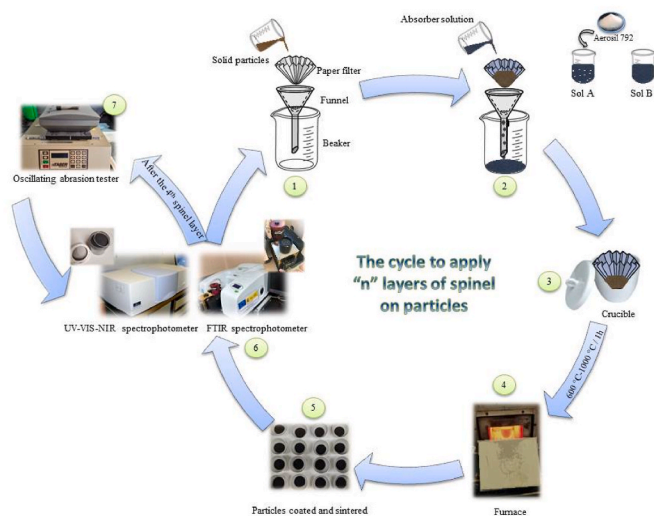


Fig. 1. Scheme of the experimental procedure followed to coat and analyse particles.

2.2. Abrasion test

An adapted Taber oscillating abrasion tester (Model 6160) has been used to evaluate the effect of abrasion due to interactions between the particles. This equipment was originally designed to rub the sample under study with an abrasive agent such as sand or other compound that acts as abrasive [41]. As in the case of the particles, this original procedure cannot be followed and the abrasive agent itself is the interactions between the particles, a pad with three compartments for test tubes has been introduced in the original device in order to test several samples at the same time. Three glass tubes filled with 7 mL of coated particles (Gen3) were subjected to the cyclic oscillating movement. The cycle speed applied was 100 cycles per minute, accumulating several cycles up to a maximum of 16,000. From time to time, the particles were removed and optically characterised.

2.3. Optical and structural characterisations

The hemispherical reflectance spectra of solid particles were measured by a UV-VIS-NIR PerkinElmer Lambda 950 double beam spectrophotometer equipped with a 150 mm Spectralon coated integrating sphere. The wavelength range used was from 0.3 to 2.5 μm . Given the challenging requirement of placing the samples in a vertical position for their optical measurements on the spectrophotometer, the measurements of the particles were based on the Montecchi window optical model included in the SolarPACES reflectance guideline [42]. For this, the particles were poured into a sample holder equipped with a window made of quartz glass that is a material transparent in the measurement range (0.3–2.5 μm). A diffuse Spectralon coupon of 10–20 % reflectance has been used, given its similar reflectance characteristics to the particles measured. The reflectance was calculated according to the SolarPACES reflectance guideline [42] by applying Equation (1), which relates the reflectance and transmittance of the window and then calibrates the measurement with respect to the target with and without the window, subtracting them from the value of the sample.

$$R_s = \frac{\rho_{w,s} - \rho_w}{\tau_w^2 + \rho_w (\rho_{w,s} - \rho_w)} \quad (1)$$

where.

R_s is the near-normal hemispherical spectral reflectance of the specimen (the particle layer).

$\rho_{w,s}$ is the overall near-normal hemispherical reflectance spectrum of the specimen measured at the near incidence angle θ_0 through the window.

ρ_w and τ_w are near-normal hemispherical reflectance and near-normal hemispherical transmittance spectra of the window at θ_0 .

The solar-weighted hemispherical reflectance ($R_{s,h}$) was calculated according to the ASTM standard E903-20 procedure [43] by weighting the hemispherical spectral reflectance $R_s(\lambda)$ with the direct AM1.5 solar spectrum (G_b) from ASTM G173-03 [44] between 0.3 and 2.5 μm , applying Equation (2).

$$R_{s,h} = \frac{\int_{0.3}^{2.5} R_s(\lambda) \cdot G_b(\lambda) d\lambda}{\int_{0.3}^{2.5} G_b(\lambda) d\lambda} \quad (2)$$

The solar-weighted hemispherical absorptance (α_s) of the particle analysed was calculated from $1 - R_{s,h}$.

The thermal emittance (ϵ_T) at a selected temperature was also calculated following the SolarPACES reflectance guideline [42], applying Equation (3). IR-reflectance spectra of particles recorded from 2.5 to 17 μm were obtained with a PerkinElmer Frontier FTIR spectrophotometer equipped with a diffuse gold-coated integrating sphere. For the measurements, a sample holder made of ZnSe window which is a material transparent to the measurement range (2–20 μm) has been used

as well as a certified diffuse gold reference.

$$\epsilon_s(T) = \frac{\int_{2.5}^{17} [1 - R_s(\lambda)] M_{bb}(\lambda, T) d\lambda}{\int_{2.5}^{17} M_{bb}(\lambda, T) d\lambda} \quad (3)$$

where.

$\epsilon_s(T)$ is the thermal emittance of the sample at the selected temperature.

$R_s(\lambda)$ is the hemispherical spectral reflectance.

M_{bb} is the emission intensity of a black body for every wavelength at a given temperature, calculated according to Planck's law.

The thermal stability of the bare and Gen3 coated particles with four layers of Sol A spinel solution was studied by subjecting the particles at 1000 °C in a muffle furnace for up to 4000 h. Both the α_s and $\epsilon_{900\text{ °C}}$ were analysed before and after each ageing step.

The surface roughness of the layers prepared from Sol A or Sol B was studied in samples deposited on quartz substrates (thickness of 3 mm) and characterised by profilometry using a Dektak 150 Surface Profiler. Ten linear scans of 1 mm length were carried out with a pin of 2 μm diameter and a load of 3 mg. The average surface roughness (R_a) was calculated according to ISO 4287, being the data presented in this work the mean value of ten measurements per sample.

A digital microscope (Olympus DSX1000) was used to study and compare the morphology, aspect and colour of some selected coated particles. X-ray analysis of the absorber thin films was carried out with a Pananalytical XPERT X-ray diffraction spectrometer (XRD), where the crystalline phases were identified. In addition, coated particles were microstructurally and chemically analysed by SEM (Ultra 55, Zeiss, Wetzlar, Germany) and energy-dispersive spectroscopy (EDS; UltiMate, Oxford, Abingdon, UK); with cross-section preparation micro and nanoindentation.

3. Results and discussion

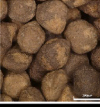
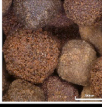
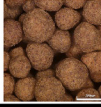
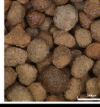
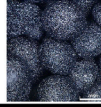
The motivation to reach the maximum α_s value, setting a 95 % minimum desirable absorptance as a positive result, led to the study of the influence of several parameters on this value. These parameters include the type and size of particles (S.O.A. and new generation), the number of spinel layers applied, the method of applying these absorbing layers and their respective sintering heat treatments and the composition of the precursor solution. The results are discussed in the next points.

3.1. Physico-chemical properties of solid particles

Four porous S.O.A particles and a new candidate of granulated particles (Gen 3), developed by Saint-Gobain, were used in this work. The so-called S.O.A particles stem from a previous activity of Saint-Gobain dedicated to the development and production of proppants, and the new granulated particles have been developed in the frame of the COMPASSCO2 project, among others. The five different types of particles have been characterised in the project in terms of the physico-chemical properties that have priority for the CSP application. Table 1 summarises the most relevant physico-chemical characteristics and the economic cost per kg, in decreasing order from the highest to the lowest importance, of the particles tested. The data designed in green refer to the physico-chemical properties that meet the requirements of the target implemented by the project consortium, whereas the red numbers reveal the ones that underperform. Data for the newly developed granulated particle Gen 3, which has a homogeneous microstructure and is made of a rich content of iron oxide that comes from recycled products from the steel industry, are not fully included in this comparative table, as it is in the process of being patented by Saint-Gobain.

Based on the data shown in Table 1, it can be seen that, depending on

Table 1
Physico-chemical properties of the tested particles.

Property	Target values	Sintered Bauxite SB 30/50	BauxLite BL 16/30	BauxLite BL 30/50	InterProp IP 30/50	Granulated Gen 3
						
Size distribution regarding performance [μm]	>1000μm (wind)	297-590	590-1190	297-590	297-590	600-1200
Cost [€/kg]	<1.5	<1.5	<1.5	<1.5	<1.5	~1
C_p at 1000 °C [J/g·K]	>1.2	1.28	1.16	1.71	1.76	
Bulk density ρ_b [g/cm ³]	>2	1.85	1.74	1.61	1.73	2.83
Material density ρ_m [g/cm ³] specific/absolute	>3.5	3.3/3.45	3.06/3.42	3.12/3.26	3.16/3.34	4.92/5.04
Softening temperature T_s [°C]	>900	882	857	850	856	1080
Vickers Hardness HV 0.1	>900	911	833	623	723	
Breaking force F [N] 0.8-1.0 mm	>140		141			
Sphericity [-] B/L (Q3=50.0%)	>0.9	0.869	0.875	0.878	0.840	
Roundness [-]	As good as bauxite		0.72	0.71	0.76	0.81
Solar absorptance α_s [-]	>0.9	0.831	0.905	0.837	0.819	0.882
Thermal emittance ε at 700 °C [-]	<0.85	0.767	0.848	0.775	0.751	0.734
		Degradation after 500 h at 1000 °C				
$\Delta\alpha_s$	<1%	-0.167	-0.131	-0.082	-0.164	+0.003
$\Delta\varepsilon_T$ (700 °C)	<1%	-0.258	-0.260	-0.173	-0.213	+0.004

the type of particle, these solid materials can have a variable α_s , density (ρ_m) and size. One of the drawbacks of the four S.O.A. proppants studied is the reduction of their α_s over time (as an example, the data of the ageing at 1000 °C during 500 h). On the contrary, the Gen 3 particles exhibit good thermal stability, withstanding the 500 h at 1000 °C without showing any alteration/loss of the α_s value due to their softening temperature around 1080 °C (Table 1). Among the S.O.A. particles, and taking the target values as a reference, the BL 16/30 particles are the ones whose properties best fit the target specifications.

Regarding the chemical composition of the bauxites of the proppants family developed by Saint-Gobain, the sintered bauxite (SB) contains the highest amounts of alumina and the lowest amounts of silica among the rest of the particles studied. Meanwhile, bauxlite (BL) is made up of the highest amounts of silica and the lowest amounts of alumina. Between these two extremes are the interprop (IP) particles, which contain the highest iron oxide quantity and intermediate amounts of alumina and silica with respect to SB and BL. These chemical variations influence the optical properties (α_s , ε_T) of the particles, as can be corroborated in Table 1 as well as their crush resistance and thermal conductivity. The

BL has the highest crush resistance (5 % at 69MPa) and the lowest thermal conductivity at high temperature (0.032 at 1000 °C), while the SB has the lowest crush resistance (0.6 % at 69MPa) and the highest thermal conductivity at high temperature together with IP (0.066 at 1000 °C).

3.2. Effect of depositing sequential Sol B-layers on S.O.A. Particles and their curing temperature

The S.O.A. solid particles were coated with a maximum of four spinel layers (Sol B) and sintered following two different heat treatments (Method 1 and Method 2) to compare, evaluate and determine the optimal conditions to reach the highest α_s value with minimal energy consumption during thermal curing. Method 1 was designed with the aim of minimising the economic costs by first sintering each deposited spinel layer at 600 °C for 1 h and then, once the fourth layer is sintered at 600 °C, performing a subsequent heat treatment at 1000 °C for 2 h. Differently, Method 2 consisted of directly sintering each deposited layer at 1000 °C for 2 h. The reason for using these high temperatures to

densify the coatings comes from the high temperatures that they would reach in operation (1000 °C). In this way, the use of temperatures similar to those reached under working conditions will ensure the maintenance of the coating properties, minimising possible future diffusion problems, layer breakage, etc.

The evolution of the α_s value as consecutive spinel layers are deposited on the S.O.A. particles is displayed in Fig. 2. As can be seen, regardless of the heat treatment applied, higher α_s values are obtained as the number of spinel layers deposited on the particles increases, reaching the maximum value with a fourth layer. However, the range of values is quite different between both heat treatments. The layers sintered at 600 °C presented a higher α_s value than those sintered at 1000 °C, since at a lower heat treatment temperature the layers are not as dense. Nonetheless, as the temperature increases from 600 °C to 1000 °C, the coating is thinner and therefore the value of α_s is reduced. By comparing the results obtained from the four-layer samples after sintering at 1000 °C with both heat treatments, it is observed that higher α_s values were obtained with Method 2 (0.958 instead of 0.917 obtained in Method 1 for BL 16/30 particles, for example). One exception is the BL 30/50 particles whose α_s value is almost the same for both heat treatments (0.956 vs. 0.953).

The differences observed in the α_s values in both heat treatments are examined in Fig. 3 where the hemispherical reflectance spectra obtained for the four accumulated coatings on the BL 16/30 particles are displayed. From this graph, a minimal difference in the reflectance value in

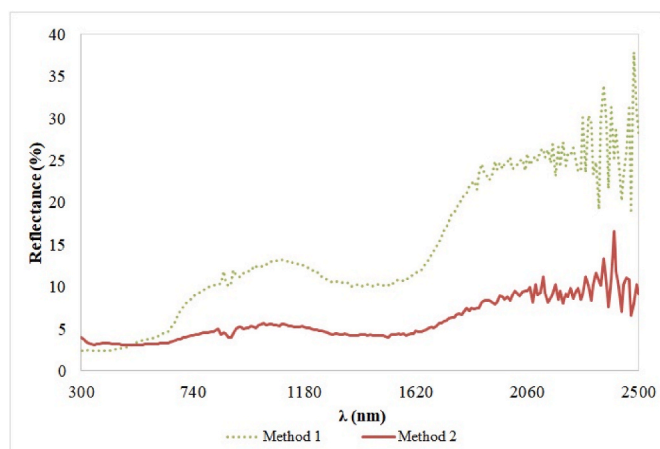
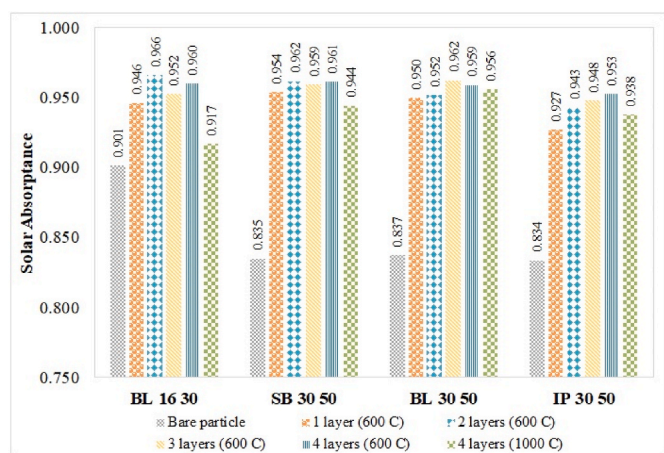


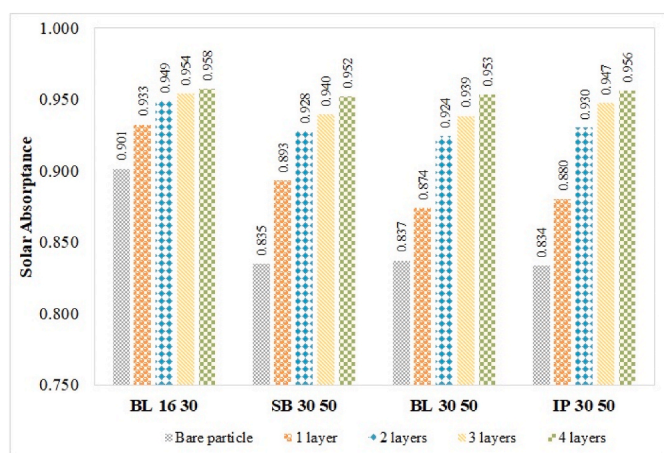
Fig. 3. Hemispherical reflectance spectra of BL 16/30 particles coated with four Sol B consecutive layers and sintered by Method 1 and Method 2.

the range comprising 300 and 500 nm is observed. The coating sintered according to Method 1 presents a lower reflectance than Method 2 but these values are within the measurement uncertainty, which is about 1 %. With respect to the wavelength range of 550–2500 nm, where the layer thickness is a determining factor, important differences can be appreciated, being attributed the lower reflectance values of Method 2 to the formation of thicker layers. At this point, it is interesting to emphasise the risk that does not allow the layers to be sufficiently sintered at 600 °C in heat treatment 1, which can consequently cause a weakening of the final coating structure. This statement coincides with what happens in dip-coating methodology when new layers are deposited on top of other less dense layers. In this case, several phenomena can occur, such as the appearance of cracks in the layers and delamination or loss of thickness due to partial ruptures of the outer parts of the layers with less density. Definitely, Method 2 benefits the formation of a thicker four-layer pack and produces a smoothing of the roughness.

Fig. 4 collects the diffraction patterns corresponding to the powder samples obtained from heating the precursor solution used to reproduce the sintering method applied to the particles. It can be seen that both sintering methods resulted in a slightly different absorbent structure that supports the differences obtained in the optical properties. Peaks well matched with the phases of CoO (JCPDS 00-042-1300), Co₃O₄ (JCPDS 04-022-7366), MnO₂ (JCPDS 04-026-2316) and CuMn₂O₄ (JCPDS 04-005-6874) appear in both spectra. However, when Method 2 is



a)



b)

Fig. 2. Effect of depositing consecutive Sol B-layers on α_s values on the porous S.O.A. Heat treatment method 1, a). Heat treatment method 2, b).

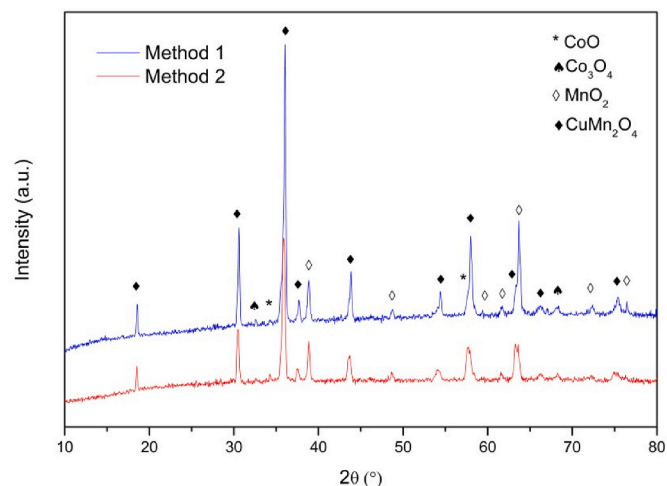


Fig. 4. XRD spectra of precursor solution powder obtained from reproducing the sintering method applied on the particles.

applied, less sharp and less intense peaks are obtained for the MnO_2 and CuMn_2O_4 phases. Nevertheless, the peaks related to the CoO phase are more intense and defined, indicating a higher presence of this crystalline compound in comparison to the Method 1. In fact, CoO is well known as a material with intrinsic high-absorption properties [45,46]. Similar structural results are obtained with samples deposited on a quartz substrate applying the same procedure.

Optical microscope images of the four consecutive absorber layers on BL 16/30 particles sintered following both heat treatments are shown in Fig. 5. The different colour of the samples is clearly appreciated. Particles sintered by Method 1 are browner, whereas those sintered by Method 2 are black. This colour difference supports the results obtained by X-rays and by the hemispherical specular reflectance measurements. The blacker the sample, the more it absorbs, which increases its α_s value.

In conclusion, the higher α_s value obtained with Method 2 heat treatment is attributed to the formation of thicker, more compact layers and with a higher presence of black CoO . From this comparative study between both heat treatments, Method 2 was selected as the optimal to perform the succeeding studies. In this way, all the deposited layers are completely sintered, seeking to ensure minimal optical ageing over time.

Completing the results obtained from the optimum heat treatment 2, in Fig. 6 is displayed the hemispherical reflectance spectra of the four S.O.A. particles coated with four layers (Sol B). As can be seen, the shape of the curve is quite similar in the range between 300 and 1700 nm for the tested particles, being the greatest difference observed in the near-IR region.

As shown in Fig. 2 b) and in relation to the heat treatment Method 2, all particles tested coated with four layers (Sol B) reached the 95 % minimum desirable α_s established as a goal. A clear increase in the α_s value is observed when going from three to four layers of spinel deposited. The highest α_s was presented by the four coated BL 16/30 particles (0.958).

Since the best results were obtained with the BL 16/30 particles,

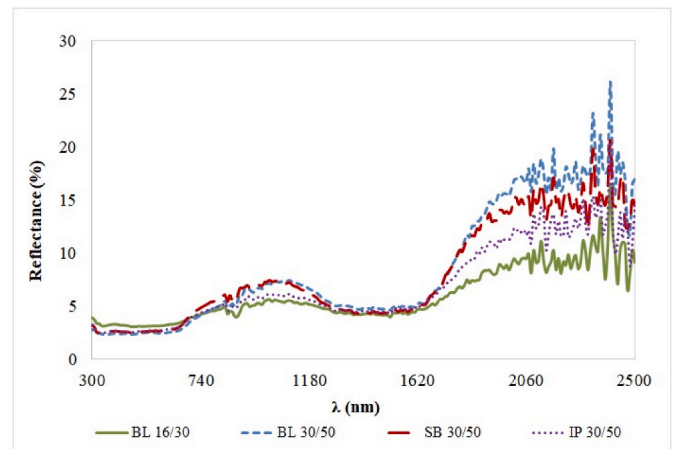


Fig. 6. Hemispherical reflectance spectra of the four studied S.O.A. particles coated with a maximum of four spinel layers.

Fig. 7 shows the graphic variation of the hemispherical reflectance from 300 to 2500 nm with the number of layers applied to these particles. As can be seen, as the solid particles are coated with the additional spinel layer, the hemispherical reflectance spectra decrease considerably, implying a thicker coating and leading to an increase in the α_s value.

The BL16/30 particles coated with four layers (Sol B) and heated with Method 2 have been characterised by the SEM-EDX technique. Fig. 8 reveals a uniform layer on the surface of proppants, with a thickness of around 3–4 μm , which is indicated by Cu-rich purple regions. Since the K, L alpha values for Mn and Fe overlap, Cu is considered as the most representative component for observing the coating. Furthermore, the typical proppant morphology comprised of main phase corundum (Al_2O_3), Fe bearing crystals and the surrounding glassy

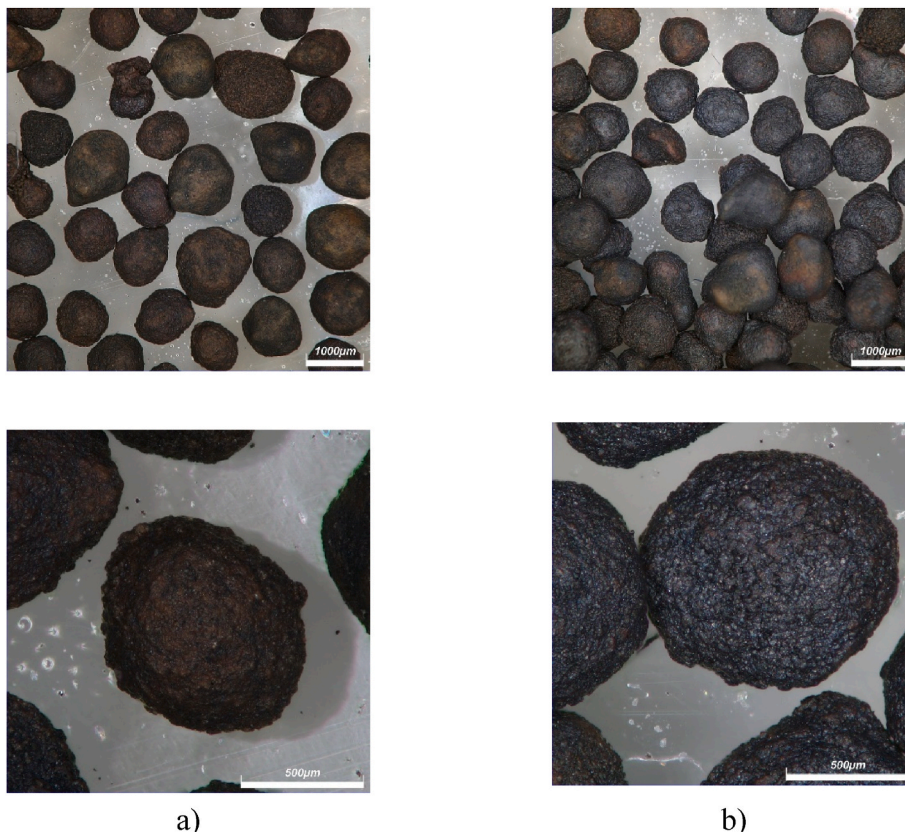


Fig. 5. Final aspect of Sol B-coated particles after heat treatment Method 1 a) and Method 2 b).

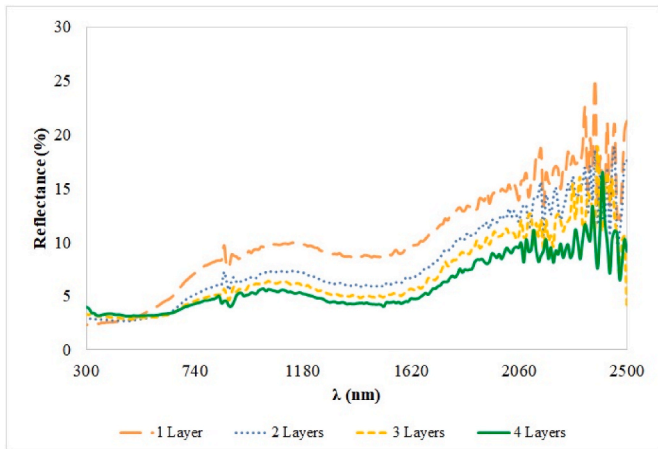


Fig. 7. Variation of the hemispherical reflectance spectra with the number of Sol B layers on the BL 16/30 particles following heat treatment Method 2.

matrix were revealed, which indicates that the inner structure remained unaffected by the coating process. It is also worth mentioning that several particles were investigated and all exhibited a microstructure similar to that presented in Fig. 8, indicating the reproducibility of the coating process.

3.3. Application of the optimised coating preparation conditions in the new Gen3 particle

The latest dense granulated Gen3 particles, whose hardness and heat capacity are improved with respect to those of the S.O.A., were coated following the same experimental procedure used for proppants, i.e. applying a maximum of four spinel coatings and employing the heat treatment method 2, in order to compare it with the S.O.A. results (Section 3.2). As can be seen in Fig. 9, when spinel layers were applied to Gen3 particles, the α_s value increased from 0.882 (bare particle) to 0.950, reaching this maximum value after the deposition of the third layer and then decreasing to 0.948 with the fourth layer. Additionally, these preliminary results showed that coated Gen3 particles achieved slightly lower α_s values than coated S.O.A. particles whose α_s values were between 0.952 and 0.958. This lower α_s value after four layers of

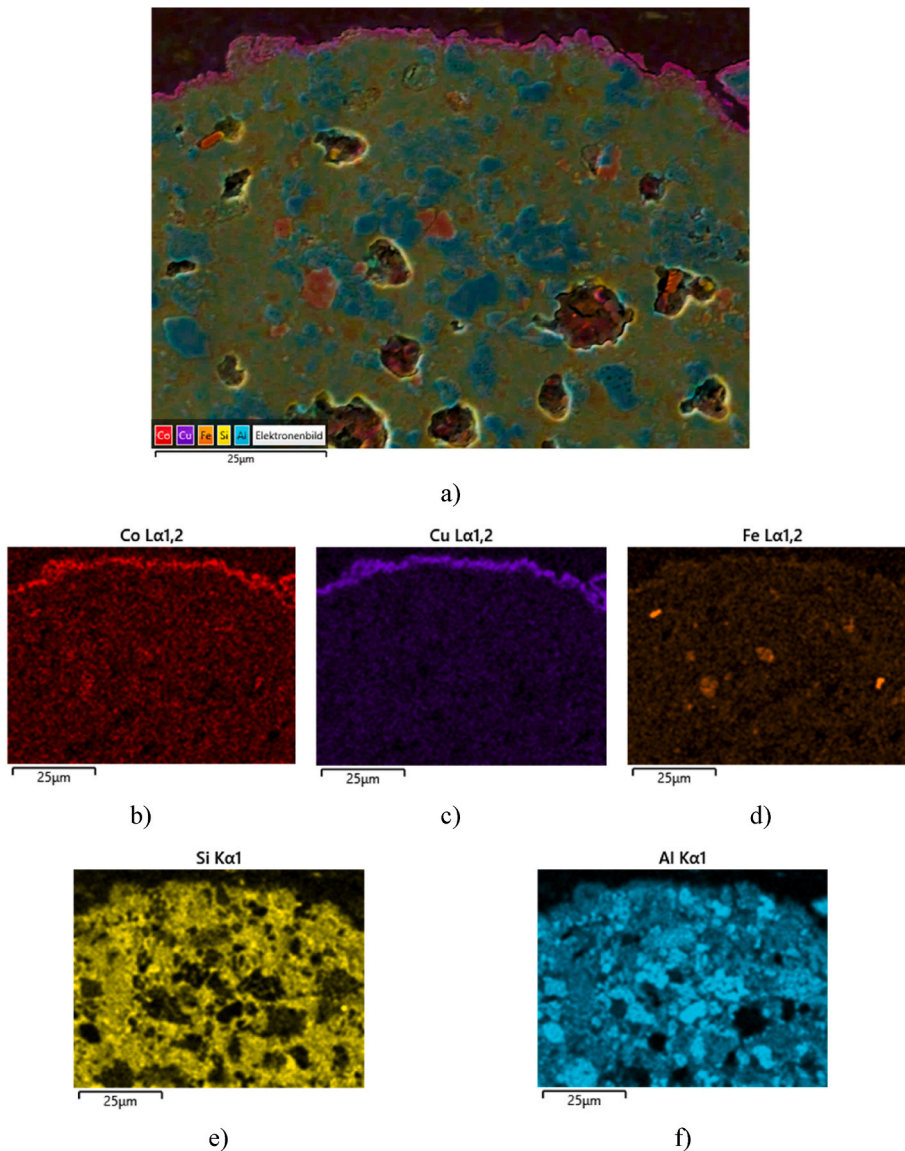


Fig. 8. SEM/EDS mapping of the BL 16/30 proppant after four layers of absorber coating (Sol B) a) with the corresponding elemental mapping of: Co b), Cu c), Fe d), Si e) and Al f).

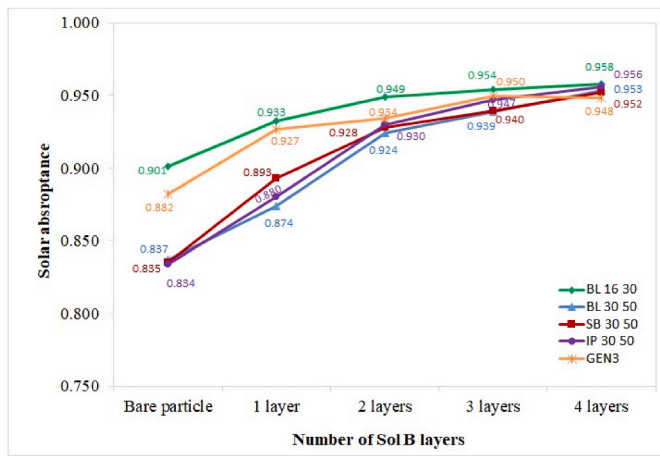


Fig. 9. Variation of the α_s value as absorber layers are deposited on tested particles following heat treatment Method 2.

spinel applied to the Gen3 particles is linked to the surface properties of this new solid candidate, which is smooth, brilliant and quite dense, as shown the microscope pictures included in Table 1, causing the precursor solution to slide more easily over the surface of the particles, retaining less liquid.

3.4. Comparison between depositing different precursor solution compositions in Gen3 particle

In order to increase α_s values and surpass those reached by the S.O.A. particles, the Gen3 particles were coated with a new spinel solution labelled as Sol A, which provides roughness to the coatings by containing silica nanoparticles in its composition. The interest in adding roughness to the layers is to promote multiple reflexions of incident solar radiation in the rough structure of the coating, intensifying the solar absorption [47]. This phenomenon is known as wave-front discrimination, and is produced when the wavelength of the incident radiation is equal to or less than the measured roughness of the coating surface. Definitely, roughness influences the solar absorption capacity of the coating in the region comprising the VIS and the NIR [48,49]. As a general trend, the increase in the roughness of the coating is accompanied by an increase in the α_s and ε_T [50,51]. Fig. 10 shows the evolution of the α_s value together with the roughness of the surface when consecutive spinel layers of Sol A (a) or Sol B (b) were applied to the substrates. The evolution of the α_s value was studied in Gen3 particles, meanwhile, the variation of the surface roughness was analysed on coated quartz substrates to rule out the influence of the substrate and analyse the behaviour of only the coating. The results depicted in Fig. 10 show that regardless of the spinel solution used, the increase in the number of spinel layers implies an increase in the α_s value up to a

maximum of four deposited layers. Furthermore, it demonstrates the higher absorbing ability of Sol A with which a α_s value of 0.949 was reached by depositing only one layer of Sol A instead of four layers in the case of applying Sol B (Fig. 10 b)). The solar absorptance value of almost 0.98 obtained with 4 layers of Sol A is remarkable. This drastic difference lies in the nature of Sol B, which produces smooth layers with a slight variation in the roughness of the coated particle as the spinel layers accumulate and therefore to very slight increases in α_s . What is observed for Sol B coincides with what was previously reported by Bergström et al. [52] i.e. for roughnesses below 150 nm, the influence of this physical magnitude on the α_s may not be as significant [50]. This statement supports the results presented in this work. The greater roughness achieved with Sol A (>150 nm) benefits from a greater increase in the α_s compared to Sol B, which presents a lower roughness of the coating. In the case of Sol A, the roughness increases considerably with the number of layers up to a maximum of four layers, providing similar roughness values with four (Ra 260 nm) and five layers (Ra 265 nm). Regarding Sol B, between two or three coats, there is hardly any change in roughness, reaching the maximum roughness (Ra 137 nm) with four layers and losing it after the application of a fifth layer (Ra 127 nm). According to the roughness values provided, Sol A gives place to a greater deviation between the measurements as more roughness is generated, giving rise to more pronounced error bars.

Fig. 11 shows the profile scans of the quartz samples as the Sol A a) and Sol B b) consecutive layers were deposited. Sol A samples present a 2D scan with numerous hills and valleys that are accentuated as the number of deposited Sol A layers increases, indicating the increase in roughness. On the contrary, the 2D scan profile of Sol B-coated samples is softer with shallow hills and valleys compared to Sol A samples. Despite the fact that the roughness values of Sol B-coated samples are lower, they also demonstrate an increase in roughness when going from three to four layers and a loss of roughness when going from four to five layers.

In addition to the conclusions reached from the roughness data, the decrease in the α_s once the fifth spinel layer is applied due to a reduction/maintenance of the roughness is corroborated in the spectra shown in Fig. 12 a) and b). In both cases, the reflectance decreases with the number of absorber layers. This result is due to two phenomena: the increase in the surface roughness that leads to light scattering and radiation loss, and the increase in coating thickness that causes high infrared absorption and higher light attenuation [53]. These findings were in agreement with other authors who reported the effect that the surface roughness and coating thickness have on the absorber optical properties [47]. Note that the reflectance spectra of the four and five-layers configurations are practically the same, suggesting that the application of more than four layers does not improve the optical properties. Thus, finding the right balance between thickness and roughness is essential to achieve the best optical properties. This balance was achieved in this work by coating the Gen 3 particles with four layers of Sol A spinel solution; achieving the best α_s value (close to 0.98) with

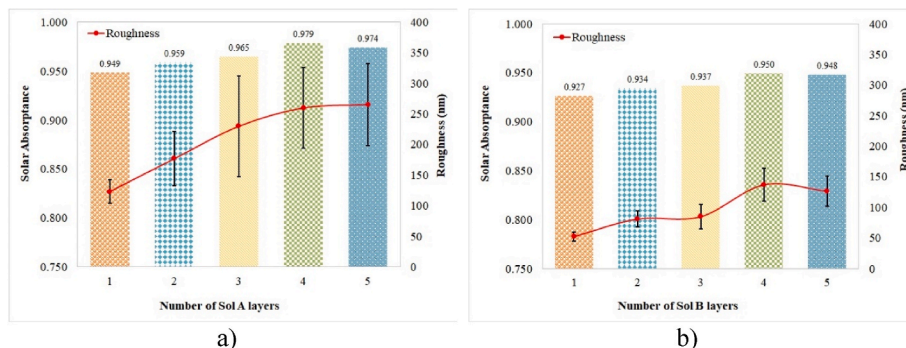
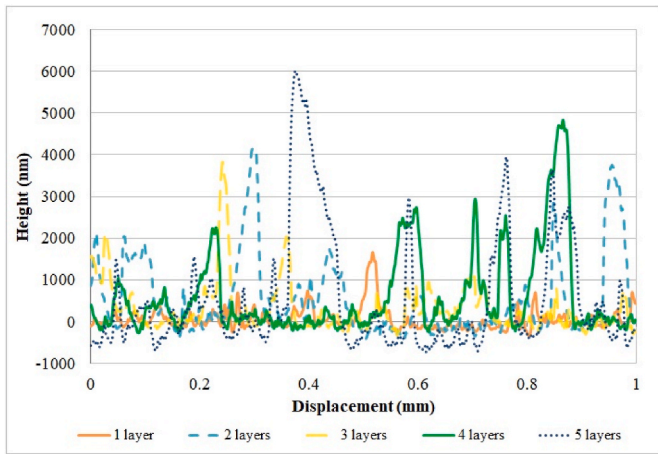
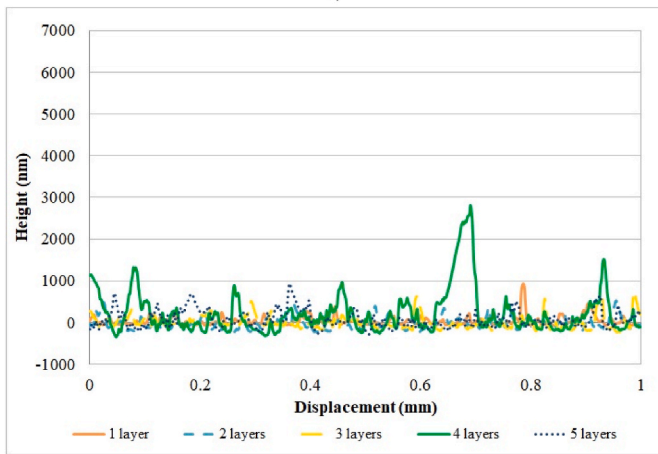


Fig. 10. Effect of both spinel composition and number of deposited layers on Gen3 particles on α_s values and surface roughness (red dot curve): Sol A a), Sol B b).



a)



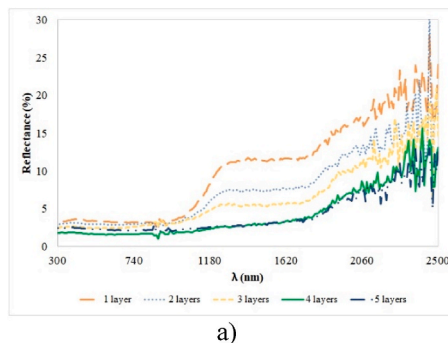
b)

Fig. 11. Variations of the 2D profile scan as Sol A a) Sol B b) spinel layers are deposited on quartz samples.

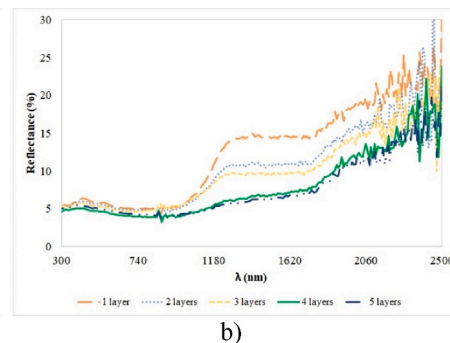
high reproducibility between different batches.

Besides, the effect of the composition of the solution on the Gen 3 particles has been studied using the SEM-EDX technique, as represented in Fig. 13. These images correspond to four-layers configuration and reveal the difference in thickness and uniformity of the absorber coating between the two solutions used.

By comparing these images, it can be seen that the Sol A-coated particles present a homogeneous spinel layer with a thickness around the submicron size stabilised on the surface, while the Sol B-coated particles show a thicker spinel layer (~25 μm) diffused also to the inner



a)



b)

Fig. 12. Variation of the hemispherical reflectance as the spinel layers Sol A a) and Sol B b) are deposited on Gen3 particles.

parts of the Gen 3 material. Furthermore, due to the difference in the compositions of the precursor solution, a clear difference in the elemental mapping of Si can be observed, as shown in Fig. 13 c) and d). The presence of silicon nanoparticles in the Sol A coating solution resulted in Si-rich regions in the coating A.

Based on these promising results obtained with Sol A and the required mechanical resistance that must present coated particles, abrasion resistance testing of coating layers was performed. Sol A and sol B coated particles were tested to compare the resistance of both absorber solutions against abrasion. Fig. 14 shows the variation of the α_s value as oscillating abrasion cycles accumulate in both types of coated Gen3, including in the inset the hemispherical reflectance spectra after 16,000 abrasion cycles accumulated for both cases.

An interesting opposite trend between both coatings has been observed from Gen3 coated particles for the first 1500 abrasion cycles. In the case of Sol A-coated particles, a marked decay of the α_s value (from 0.974 to 0.969) has been noticed while, in contrast, Sol B-coated particles registered a considerable increase in the α_s value (from 0.940 to 0.953). The decay of the α_s value of the Sol A-coated particles is consequence of erosion between the particles, which causes a reduction in the thickness of the absorber coating. In the case of Sol B-coated particles, a combined effect took place due, on the one hand, to the reduction of the film thickness and, on the other hand, to the erosion of the absorber film, which increases the roughness of the particles leading to an initial increase in the α_s . In both cases, from 1500 abrasion cycles the loss of thickness of the absorber coating as a consequence of the accumulated erosion causes the α_s to decrease asymptotically with the number of cycles. A α_s value of 0.963 were reached for Sol A-coated particles after 16,000 abrasion cycles, while a α_s value of 0.947 was obtained for Sol B-coated Gen3 particles. This comparative behaviour highlights that the particles coated with Sol A gradually lose their absorptance optical properties as the coating is lost due to abrasion, but they maintain acceptable conditions to continue perfectly operating.

Fig. 15 shows the variation of the hemispherical reflectance spectra with the cumulative number of abrasion cycles for the Sol A-coated particles. Given the large number of spectra, only the complete spectra obtained in some selected numbers of abrasion cycles are plotted, although the absorptance values for all cycles are collected in Fig. 14. The hemispherical reflectance spectra shows an increase in solar reflectance throughout the solar wavelength range because of a reduction in coating roughness and a loss of coating thickness as the abrasion cycles accumulate.

The evolution of the reflectance value is shown in more detail in Fig. 16 where at selected wavelengths (covering the entire solar range up to 1800 nm to rule out noise from the measurement equipment) the effect of accumulated abrasion cycles on the reflectance value of the particles is displayed. At 400 nm, a clear decrease in the reflectance value is appreciated since the first 200 abrasion cycles and continues to decrease as the abrasion cycles accumulate as a consequence of the reduction of the roughness of the coating. At higher wavelength values,

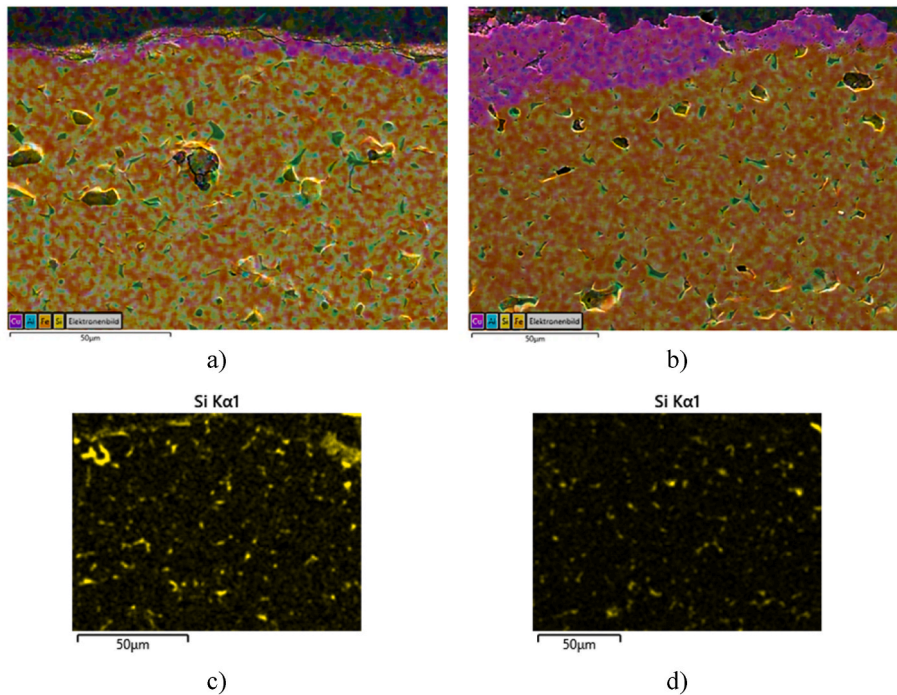


Fig. 13. SEM/EDS mapping of Gen3 particles with Sol A a) and Sol B b) coatings with the corresponding elemental Si mapping Sol A c) Sol B d).

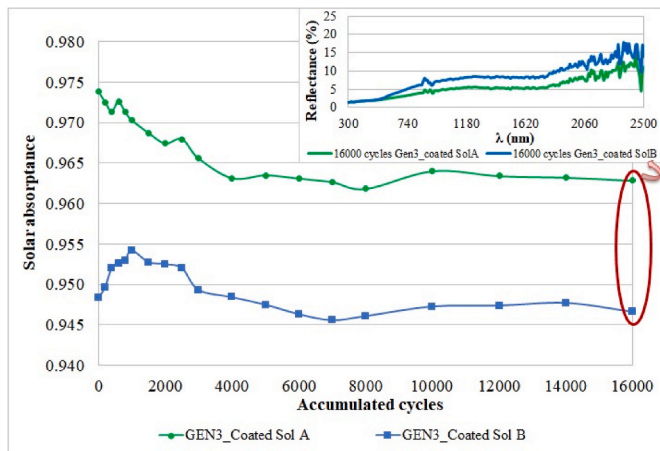


Fig. 14. Variation of the α_s value with the number of abrasion cycles in Sol A and Sol B coated Gen3 particles. Hemispherical reflectance spectra of coated particles after 16,000 abrasion cycles (inset).

i.e. 800, 1200, 1500 and 1800 nm, a drastic increase in the reflectance value is observed as the abrasion cycles accumulate as a result of the coating thickness loss.

After the large number of test cycles, the α_s values obtained are still values much higher than those presented by the uncoated Gen3 particles (0.882), showing the good resistance of the coating to abrasion between particles. After 16,000 abrasion cycles, the α_s value has only dropped around 1.1 % (α_s 0.963). This value highlights the important role that the coating plays in the final efficiency of this material.

The promising results obtained for Sol A-coated Gen3 particles raised interest in studying their thermal stability. To this end, the uncoated and coated Gen3 particles were subjected to isothermal annealing at 1000 °C for a total of 4000 h. The variation of both α_s and $\epsilon_{900^\circ\text{C}}$ are shown in Fig. 17. As can be seen, the Gen 3 particles proved to be very stable, maintaining their initial optical properties at the end of the 4000 h of testing ($\alpha_s \approx 0.883$, $\epsilon_{900^\circ\text{C}} = 0.72$). Regarding the coated Gen 3 particles,

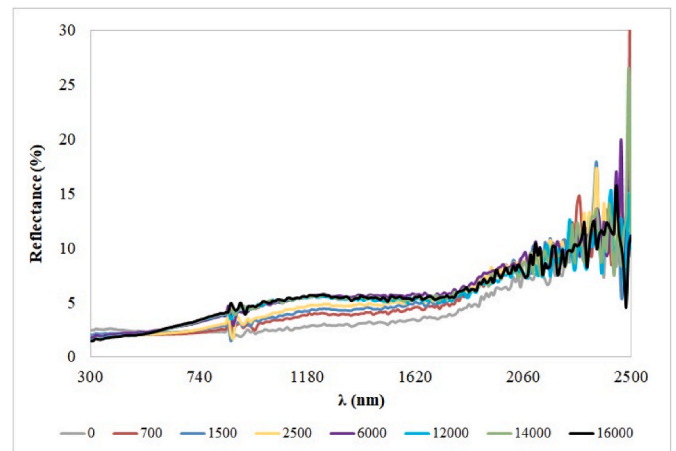


Fig. 15. Variation of the hemispherical reflectance spectra of Sol A-coated Gen3 particles in the solar range with abrasion cycles.

the coatings also showed good stability, without showing drastic degradation. Specifically, the value of α_s was only reduced by 2.5 %, from 0.975 to 0.951, and the $\epsilon_{900^\circ\text{C}}$ remained unchanged ($\epsilon_{900^\circ\text{C}}$ 0.86) after 4000 h at 1000 °C. Despite the decrease in α_s at the end of the thermal stability test, the coated particles still have an absorbance value greater than the uncoated particles (7.8 %). The value of α_s of 0.951 at the end of the test still meets the desirable absorbance set as a goal at the beginning of the project, highlighting the good quality of the coated particles that can continue to operate perfectly and ensure the thermal efficiency of the system. Definitely, both the particles and the coatings manifested good thermal stability after such a long-term thermal exposure.

4. Conclusions

Five different particles (four S.O.A. and a new granulated candidate Gen3) developed by Saint-Gobain in the frame of the COMPASSCO2

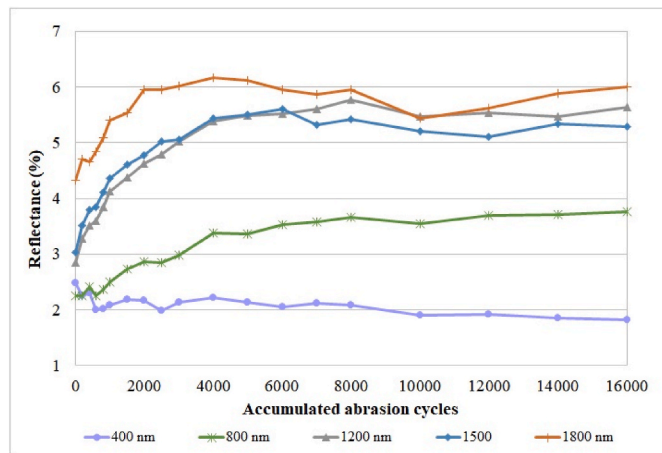
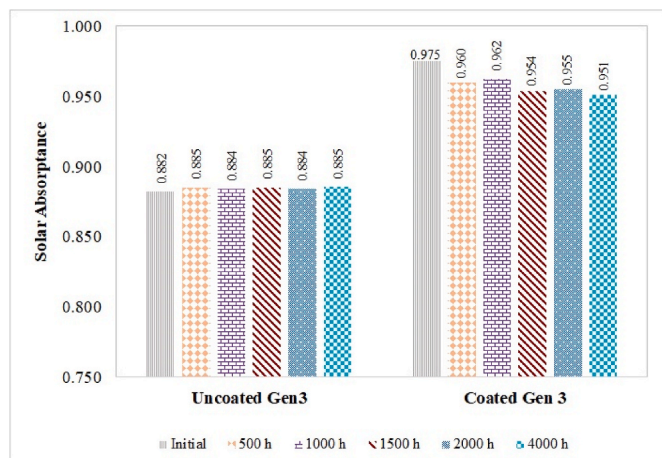
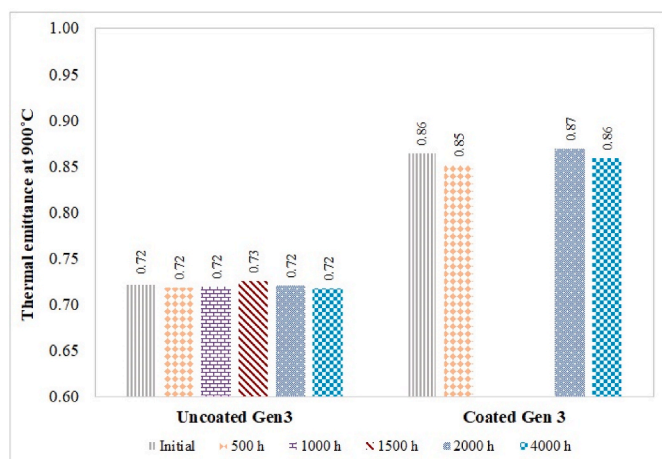


Fig. 16. Evolution of the reflectance value of Sol A-coated Gen3 particles at selected wavelengths (400, 800, 1200, 1500 and 1800 nm) as the abrasion cycles accumulate.



a)



b)

Fig. 17. Evolution of the values of α_s a) and $\epsilon_{900\text{ °C}}$ b) for uncoated and Sol A-coated Gen 3 particles during the thermal stability test at 1000 °C.

project have been employed to study their coating deposition to modify and over perform their optical properties and efficiency. A new methodology that has been adapted to the principle of dip-coating has been designed and tuned. The composition of both solid particles and

precursor solutions, the deposition of consecutive absorber layers on solid particles and their curing conditions showed a direct influence on the final α_s value, thermal stability and abrasion resistance. As the number of layers deposited increases, up to a total of four, higher α_s values are obtained reaching the maximum value by sintering each layer at 1000 °C for 2 h. The best α_s results obtained with S.O.A. particles, were obtained with BL 16/30 reaching a value of 0.952, which exceeds the 95 % minimum desirable absorptance set by the project. The addition of silica nanoparticles to the spinel precursor solution provided roughness to the final coating, affecting the resultant optical properties. Solar absorptance values up to 0.98 were achieved in the novel granulated particles. In addition, these samples presented an excellent thermal stability and good resistance to abrasion. After 4000 h of isothermal annealing at 1000 °C, the α_s value was only reduced by 2.5 % presenting the still competent value of 0.951. With regards to the $\epsilon_{900\text{ °C}}$ it remained unchanged (0.86). Also, the α_s value has only dropped around 1.1 % (α_s 0.963) after 16,000 accumulated abrasion cycles, maintaining acceptable conditions to continue operating with high performance. Therefore, this work proves the possibility of depositing dark-coloured transition-metal oxides with spinel-like structure coatings on all the particles studied, achieving the best results with the novel granulated particles coated with spinel/silica layers, being successfully met the requirements of high α_s , thermal stability and abrasion resistance.

Funding and acknowledgements

This research received funding from the European Union’s Horizon 2020 Research and Innovation Action (RIA) under grant agreement No. 958418. COMPASSCO2 project. The authors would like to thank Saint-Gobain for supplying particles for the study conducted in this paper and the information related to them and Nuria Germán and Raúl Tordeillas for their contribution in the laboratory tasks.

CRedit authorship contribution statement

Meryem Farchado: Writing – review & editing, Writing – original draft, Visualization, Validation, Methodology, Investigation, Formal analysis, Data curation, Conceptualization. **Gema San Vicente:** Writing – review & editing, Project administration, Methodology, Conceptualization. **Naia Barandica:** Writing – review & editing, Formal analysis, Investigation. **Florian Sutter:** Data curation, Formal analysis, Investigation. **Gözde Alkan:** Writing – review & editing, Investigation. **Daniel Sánchez-Señorán:** Writing – review & editing, Formal analysis, Investigation. **Ángel Morales:** Writing – review & editing, Supervision, Methodology, Conceptualization.

Declaration of competing interest

The authors declare that they have no known competing financial interests or personal relationships that could have appeared to influence the work reported in this paper.

Data availability

Data will be made available on request.

Appendix A. Supplementary data

Supplementary data to this article can be found online at <https://doi.org/10.1016/j.solmat.2023.112681>.

References

- [1] Speech by Commissioner Arias Ca Ete, A Renewable Energy Union, 2015.
- [2] A. Palacios, A. Calderón, C. Barreneche, J. Bertomeu, M. Segarra, A.I. Fernández, Study on solar absorptance and thermal stability of solid particles materials used as

- TES at high temperature on different aging stages for CSP applications, *Sol. Energy Mater. Sol. Cell.* 201 (2019), 110088.
- [3] C.K. Ho, A review of high-temperature particle receivers for concentrating solar power, *Appl. Therm. Eng.* 109 (2016) 958–969.
- [4] C.K. Ho, B.D. Iverson, Review of high-temperature central receiver designs for concentrating solar power, *Renew. Sustain. Energy Rev.* 29 (2014) 835–846.
- [5] S.G. R. Buck, Solar tower system temperature range optimization for reduced LCOE, in: *AIP Conference Proceedings*.
- [6] B.H. Mills, C.K. Ho, N.R. Schroeder, R. Shaeffer, H.F. Laubscher, K.J. Albrecht, Design evaluation of a next-generation high-temperature particle receiver for concentrating solar thermal applications, *Energies* 15 (2022) 1657.
- [7] *Concentrating Solar Power Technology Principles, Developments, and Applications*, second ed. ed., 2021.
- [8] A. El-Leathy, S. Jeter, H. Al-Ansary, S.N. Danish, R. Saeed, S. Abdel-Khalik, M. Golob, E. Djajadiwinata, Z. Al-Suhaibani, Thermal performance evaluation of lining materials used in thermal energy storage for a falling particle receiver based CSP system, *Sol. Energy* 178 (2019) 268–277.
- [9] Z. Ma, G. Glatzmaier, M. Mehos, Fluidized bed technology for concentrating solar power with thermal energy storage, *J. Sol. Energy Eng.* 136 (2014).
- [10] T. Baumann, S. Zunft, Properties of granular materials as heat transfer and storage medium in CSP application, *Sol. Energy Mater. Sol. Cell.* 143 (2015) 38–47.
- [11] C.K. Ho, Advances in central receivers for concentrating solar applications, *Sol. Energy* 152 (2017) 38–56.
- [12] C. Ho, J. Christian, D. Gill, A. Moya, S. Jeter, S. Abdel-Khalik, D. Sadowski, N. Siegel, H. Al-Ansary, L. Amsbeck, B. Gobereit, R. Buck, Technology advancements for next generation falling particle receivers, *Energy Proc.* 49 (2014) 398–407.
- [13] T. Galiullin, B. Gobereit, D. Naumenko, R. Buck, L. Amsbeck, M. Neises-von Puttkamer, W.J. Quadackers, High temperature oxidation and erosion of candidate materials for particle receivers of concentrated solar power tower systems, *Sol. Energy* 188 (2019) 883–889.
- [14] L. Sang, K. Wang, R. Zhang, Y. Wang, Y. Wu, Effective thermal conductivity and thermal cycling stability of solid particles for sCO₂ CSP applications, *Sol. Energy Mater. Sol. Cell.* 242 (2022), 111764.
- [15] L. Heller, D. Többen, T. Hirsch, R. Buck, The cost-saving potential of next-generation particle technology CSP with steam cycles, *Sol. Energy* 263 (2023), 111954.
- [16] C.B. Alejandro Calderón, Anabel Palacios, Mercè Segarra, Cristina Prieto Sanchez, A. Inés Fernández, Review of solid particle materials for heat transfer fluid and thermal energy storage in solar thermal power plants, *Energy Storage* 1 (2019) e63.
- [17] J. Chen, V.M. Wheeler, B. Liu, A. Kumar, J. Coventry, W. Lipiński, Optical characterisation of alumina–mullite materials for solar particle receiver applications, *Sol. Energy Mater. Sol. Cell.* 230 (2021), 111170.
- [18] G. Alkan, P. Mechnich, J. Pernerpointner, Improved performance of ceramic solar absorber particles coated with black oxide pigment deposited by resonant acoustic mixing and reaction sintering, *Coatings* 12 (2022) 757.
- [19] N. Siegel, M. Gross, C. Ho, T. Phan, J. Yuan, Physical properties of solid particle thermal energy storage media for concentrating solar power applications, *Energy Proc.* 49 (2014) 1015–1023.
- [20] V.P.P.d. Campos, E.C. Sansone, G.F.B.L.e. Silva, Hydraulic fracturing proppants, *Cerâmica* 64 (2018) 219–229.
- [21] F. Liang, M. Sayed, G.A. Al-Muntasheri, F.F. Chang, L. Li, A comprehensive review on proppant technologies, *Petroleum* 2 (2016) 26–39.
- [22] N.P. Siegel, M.D. Gross, R. Coury, The development of direct absorption and storage media for falling particle solar central receivers, *J. Sol. Energy Eng.* 137 (2015).
- [23] J. Roop, S. Jeter, S.I. Abdel-Khalik, C.K. Ho, Optical properties of select particulates after high-temperature exposure, in: *ASME 2014 8th International Conference on Energy Sustainability Collocated with the ASME 2014 12th International Conference on Fuel Cell Science, Engineering and Technology*, 2014.
- [24] K.K. Phani Kumar, S. Mallick, S. Sakthivel, Nanoparticles based single and tandem stable solar selective absorber coatings with wide angular solar absorptance, *Sol. Energy Mater. Sol. Cell.* 242 (2022), 111758.
- [25] M. Farchado, J.M. Rodríguez, G. San Vicente, N. Germán, A. Morales, Optical parameters of a novel competitive selective absorber for low temperature solar thermal applications, *Sol. Energy Mater. Sol. Cell.* 178 (2018) 234–239.
- [26] S.R. Atchuta, S. Sakthivel, H.C. Barshilia, Transition metal based Cu_xNi_yCo_z-x-yO₄ spinel composite solar selective absorber coatings for concentrated solar thermal applications, *Sol. Energy Mater. Sol. Cell.* 189 (2019) 226–232.
- [27] D.E. Karas, J. Byun, J. Moon, C. Jose, Copper-oxide spinel absorber coatings for high-temperature concentrated solar power systems, *Sol. Energy Mater. Sol. Cell.* 182 (2018) 321–330.
- [28] P.G. Ma, Gang Qingfen Liu, Photothermal Conversion Applications of the Transition Metal (Cu, Mn, Co, Cr, and Fe) Oxides with Spinel Structure, 2017.
- [29] A. Amri, Z.T. Jiang, T. Pryor, C.-Y. Yin, S. Djordjevic, Developments in the synthesis of flat plate solar selective absorber materials via sol–gel methods: a review, *Renew. Sustain. Energy Rev.* 36 (2014) 316–328.
- [30] A.L. Avila-Marin, A. Morales, R. Monterreal, J. Fernandez-Reche, Non-selective coating for porous materials used for solar thermal applications, *AIP Conf. Proc.* (2019) 2126.
- [31] L.A. Birgit Gobereit, Christoph happich, martin schmücker, michael wolff, assesment and improvement of optical properties of particles for solid particle receiver, in: *PowerEnergy2017-3102*, Charlotte, NC, USA, 2017.
- [32] K. Niranjana, A. Soum-Glaude, A. Carling-Plaza, S. Bysakh, S. John, H.C. Barshilia, Extremely high temperature stable nanometric scale multilayer spectrally selective absorber coating: emissivity measurements at elevated temperatures and a comprehensive study on ageing mechanism, *Sol. Energy Mater. Sol. Cell.* 221 (2021), 110905.
- [33] K. Xu, M. Du, L. Hao, J. Mi, Q. Yu, S. Li, A review of high-temperature selective absorbing coatings for solar thermal applications, *Journal of Materiomics* 6 (2020) 167–182.
- [34] S.R. Atchuta, S. Sakthivel, H.C. Barshilia, Selective properties of high-temperature stable spinel absorber coatings for concentrated solar thermal application, *Sol. Energy* 199 (2020) 453–459.
- [35] K. Tsuda, Y. Murakami, J.F. Torres, J. Coventry, Development of high absorption, high durability coatings for solar receivers in CSP plants, *AIP Conf. Proc.* 2033 (2018), 1 040039.
- [36] K.M. Chung, R. Chen, Black coating of quartz sand towards low-cost solar-absorbing and thermal energy storage material for concentrating solar power, *Sol. Energy* 249 (2023) 98–106.
- [37] L. Sang, K. Wang, Y. Wu, C. Ma, The improved solar weighted absorptance and thermal stability of desert sand coated with transition metal oxides for direct particle receiver, *Sol. Energy Mater. Sol. Cell.* 251 (2023), 112158.
- [38] J. Wu, J. Du, J. Wu, X. Du, Modification of high temperature radiation absorption properties of solid particles with surface coating, *Sol. Energy Mater. Sol. Cell.* 263 (2023), 112567.
- [39] S.M.a.I. Amirouche, *New Material Solutions from Saint-Gobain for Thermal Energy Storage*, 2021.
- [40] A. Morales, *Process to Deposit Metal and Metal Oxide Coatings*, 2003.
- [41] G. San Vicente, N. Germán, M. Farchado, A. Morales, P. Santamaría, A. Fernández-García, Study of abrasion tests for antireflective and antisoiling/antireflective coatings on glass solar tubes, *Sol. Energy* 252 (2023) 134–144.
- [42] J.P.F. Sutter, S. Caron (Dir, A. Morales, G. San Vicente, A. FernándezGarcía (CIEMAT), M. Montecchi (ENEA), A. Calderón, M. Majó, I. Fernández (Universitat Barcelona), P. Davenport, T. Farrell (NREL), C. Ho (SANDIA), Method to Evaluate the Reflectance, Absorptance and Emittance of Particles for Concentrating Solar Power Technology, 2022.
- [43] ASTM E903-20, Standard Test Method for Solar Absorptance, Reflectance, and Transmittance of Materials Using Integrating Spheres, 2020.
- [44] ASTM G173-03, Standard Tables for Reference Solar Spectral Irradiances: Direct Normal and Hemispherical on 37° Tilted Surface, 2020.
- [45] M.G. Grebenik, Comparison of different forms of black cobalt selective solar absorber surfaces, *Sol. Energy Mater.* 16 (1987) 113–131.
- [46] X.L. Zhang, J.J. Zhou, W.D. Fu, L. Chen, Research on materials of solar selective absorption coating based on the first principle, *Open Phys.* 19 (2021) 477–485.
- [47] G.G. Welegerg, Z.M. Mehabaw, H.G. Gebretisae, M.G. Tsegay, L. Kotsedi, Z. Khumalo, N. Matinisie, Z.T. Aytuna, S. Mathur, Z.Y. Nuru, S. Dube, M. Maaza, Electrodeposition of nanostructured copper oxide (CuO) coatings as spectrally solar selective absorber: structural, optical and electrical properties, *Infrared Phys. Technol.* 133 (2023), 104820.
- [48] J.V.F.F.d. Medeiros, A.d.S. Oliveira, G.O. Galvão, I.D.M.d. Medeiros, K.C. Gomes, Effect of electrodeposition time on absorptance, roughness and thermal stability of black chromium absorbing surfaces, *Mater. Res.* 25 (2022).
- [49] A. Hall, K.V. Every, M. Knight, J. McCloskey, D. Urrea, A. Ambrosini, T. Lambert, N. Siegel, A. Mahoney, C. Ho, Solar selective coatings for concentrating solar power central receivers, in: *ITSC2011*, 2011, pp. 347–350.
- [50] N. Chomcharoen, T. Muangnapoh, B. Traipattanakul, K. Surawathanawises, Improvement of optical properties of AISI 304 as a solar absorber using a pulsed fiber laser, *RSC Adv.* 13 (2023) 22281–22286.
- [51] K. Dornelles, V. Roriz, M. Roriz, Determination of the Solar Absorptance of Opaque Surfaces, 2007.
- [52] D. Bergström, J. Powell, A.F.H. Kaplan, A ray-tracing analysis of the absorption of light by smooth and rough metal surfaces, *J. Appl. Phys.* 101 (2007), 113504.
- [53] G.G. Welegerg, H.G. Gebretisae, M.G. Tsegay, Z.Y. Nuru, S. Dube, M. Maaza, Thickness dependent morphological, structural and optical properties of SS/CuO nanocoatings as selective solar absorber, *Infrared Phys. Technol.* 113 (2021), 103619.